The Astrophysical Journal, 620:223–237, 2005 February 10

INVESTIGATING THE POSSIBLE ANOMALY BETWEEN NEBULAR AND STELLAR OXYGEN ABUNDANCES IN THE DWARF IRREGULAR GALAXY WLM[1]

Henry Lee,[2] Evan D. Skillman,[2] and Kim A. Venn[2,3]
Received 2004 July 16; accepted 2004 October 26

ABSTRACT

We obtained new optical spectra of 13 H II regions in WLM with EFOSC2; oxygen abundances are derived for nine H II regions. The temperature-sensitive [O III] λ4363 emission line was measured in two bright H II regions, HM 7 and HM 9. The direct oxygen abundances for HM 7 and HM 9 are $12 + \log(\mathrm{O/H}) = 7.72 \pm 0.04$ and 7.91 ± 0.04, respectively. We adopt a mean oxygen abundance of $12 + \log(\mathrm{O/H}) = 7.83 \pm 0.06$. This corresponds to $[\mathrm{O/H}] = -0.83$ dex, or 15% of the solar value. In H II regions where [O III] λ4363 was not measured, oxygen abundances derived with bright-line methods are in general agreement with direct values of the oxygen abundance to an accuracy of about 0.2 dex. In general, the present measurements show that the H II region oxygen abundances agree with previous values in the literature. The nebular oxygen abundances are marginally consistent with the mean stellar magnesium abundance ($[\mathrm{Mg/H}] = -0.62$). However, there is still a 0.62 dex discrepancy in oxygen abundance between the nebular result and the A-type supergiant star WLM 15 ($[\mathrm{O/H}] = -0.21$). Nonzero reddening values derived from Balmer line ratios were found in H II regions near a second H I peak. There may be a connection between the location of the second H I peak, regions of higher extinction, and the position of WLM 15 on the eastern side of the galaxy.

Subject headings: galaxies: abundances — galaxies: dwarf — galaxies: evolution — galaxies: individual (WLM) — galaxies: irregular

1. INTRODUCTION

Dwarf galaxies are thought to be the building blocks in the assembly of more massive galaxies within the hierarchical picture of structure formation. These galaxies are also very important venues in which questions about cosmology, galaxy evolution, and star formation may be answered. Dwarf irregular galaxies are relatively low mass, gas-rich, metal-poor, and are presently forming stars as shown by their H II regions, whereas low-mass dwarf spheroidal galaxies are gas-poor and no longer host present-day star-forming events. The properties of these galaxies may be similar to those found in the early universe, and dwarf irregular galaxies may possibly be sites out of which damped Lyα absorber systems form at high redshift (e.g., Calura et al. 2003; Prochaska et al. 2003). An important question that has yet to be fully explained is the relationship between dwarf irregular and dwarf spheroidal galaxies (e.g., Grebel et al. 2003; Skillman et al. 2003a, 2003b; van Zee et al. 2004 and references therein). That streams have been observed within the Galaxy and M31 (e.g., Yanny et al. 2003; Martin et al. 2004; Zucker et al. 2004a, 2004b) has been taken as evidence of ongoing accretion and of past merging of dwarfs by the more massive galaxies. However, work presented by Tolstoy et al. (2003) and Venn et al. (2004a) has shown that stars in present-day dwarf spheroidal galaxies cannot make up the dominant stellar populations in the halo, bulge, or the thick disk of the Galaxy, although the merging of dwarf galaxies at very early times cannot be ruled out.

The measurements of element abundances provide important clues to understanding the chemical history and evolution of galaxies. In star-forming dwarf galaxies, the analysis of bright nebular emission lines from the spectra of H II regions is used to derive abundances of α-elements (i.e., oxygen) in the ionized gas (see, e.g., Dinerstein 1990; Skillman 1998; Garnett 2004). However, a limited number of elements can be studied by comparison with the number of elements found in the absorption spectra of stars. For a more complete picture, additional elements should be included, since various elements arise from different sites and involve different timescales. Oxygen and other α-elements are created in very massive progenitor stars before being returned to the interstellar medium (ISM) on short timescales, when these stars explode as Type II supernovae. Iron is an element produced by explosive nucleosynthesis in Type I supernovae from low-mass progenitor stars on longer timescales and is also produced in Type II supernovae. Because of the varying timescales for stars of different masses, the α-element–to–iron abundance ratio, $[\alpha/\mathrm{Fe}]$,[4] is tied very strongly to the star formation history (e.g., Gilmore & Wyse 1991; Matteucci 2003). Interestingly, $[\alpha/\mathrm{Fe}]$ values for three dwarf irregular galaxies are near or at solar, which indicates that stars have been forming at a very low rate and/or the last burst of star formation occurred long ago (Venn et al. 2001, 2003; Kaufer et al. 2004). Izotov & Thuan (1999) claim that O/Fe is elevated in low-metallicity blue compact dwarf galaxies ($[\mathrm{O/Fe}] = +0.32 \pm 0.11$). However, their analysis does not account for potential depletion of Fe onto dust grains, and the Fe abundance is only measured in Fe^{+2}, requiring very large and uncertain ionization correction factors (ICFs). Rodríguez (2003) finds that the adopted ICFs underestimate the total Fe abundance by factors larger than the elevated abundance ratio claimed by Izotov & Thuan (1999). Thus, it is prudent to assume that the nebular Fe abundances in these galaxies, and thus the nebular O/Fe ratios, are quite uncertain (Garnett 2004). At present, reliable O/Fe ratios will need to be obtained from

[1] Based on EFOSC2 observations collected at the European Southern Observatory, Chile; proposal No. 71.D-0491(B).

[2] Department of Astronomy, University of Minnesota, 116 Church Street SE, Minneapolis, MN 55455; hlee@astro.umn.edu, skillman@astro.umn.edu.

[3] Department of Physics and Astronomy, Macalester College, 1600 Grand Avenue, Saint Paul, MN 55105; venn@macalester.edu.

[4] We use the notation $[\mathrm{X/Y}] = \log(\mathrm{X/Y}) - \log(\mathrm{X/Y})_{\odot}$.

stellar abundances. While a complete discussion of α/Fe values is beyond the scope of the present work, brief reviews of stellar abundances in external galaxies have recently been presented by Tolstoy & Venn (2005) and Venn et al. (2004b).

High-efficiency spectrographs on 8 and 10 m telescopes have made possible the spectroscopic measurement of individual stars in extragalactic systems. In particular, bright blue supergiants have been observed in galaxies at distances of about 1 Mpc. These hot young massive stars allow us to measure simultaneously present-day α- and iron-group elements. The important advantage of these measurements is that they also allow for the direct comparison of stellar α-element abundances with nebular measurements, as massive stars and nebulae are similar in age and have similar formation sites. Oxygen abundances derived from the spectroscopy of blue supergiants have been obtained in nearby dwarf irregular galaxies NGC 6822, WLM, and Sextans A (Venn et al. 2001, 2003; Kaufer et al. 2004).

The relative ease with which spectra of H II regions have been obtained in dwarf irregular galaxies has led to establishing (1) the metallicity-luminosity relation, thought to be representative of a mass-metallicity relation for dwarf irregular galaxies (e.g., Skillman et al. 1989a; Richer & McCall 1995; Lee et al. 2003b); and (2) the metallicity-gas fraction relation, which represents the relative conversion of gas into stars and may be strongly affected by the galaxies' surrounding environment (e.g., Lee et al. 2003b, 2003c; Skillman et al. 2003a). It is assumed that nebular oxygen abundances are representative of the present-day ISM metallicity for an entire dwarf galaxy, where there is often only a single H II region present. In fact, spatial inhomogeneities or radial gradients in oxygen abundances have been found to be very small or negligible in nearby dwarf irregular galaxies (e.g., Kobulnicky & Skillman 1996, 1997), although recent observations have cast uncertainty on the assumption in NGC 6822 and WLM (Venn et al. 2001, 2003). Here we focus on oxygen abundances and the comparison between stellar and nebular determinations. For the remainder of this paper, we adopt $12 + \log(\mathrm{O/H}) = 8.66$ as the solar value for the oxygen abundance (Asplund et al. 2004).

1.1. *WLM*

WLM (Wolf-Lundmark-Melotte) is a dwarf irregular galaxy at a distance of 0.95 Mpc (Dolphin 2000) and is located in the Local Group. The galaxy was discovered by Wolf (1910)[5] and independently rediscovered by Lundmark and Melotte (Melotte 1926). WLM is relatively isolated, as the nearest neighbor, about 175 kpc distant, is the recently discovered Cetus dwarf spheroidal galaxy (Whiting et al. 1999). Basic properties of the galaxy are listed in Table 1.

A number of observations are summarized here. Jacoby & Lesser (1981) identified two planetary nebulae in the galaxy, and Sandage & Carlson (1985) identified the brightest blue and red supergiant stars, including over 30 variable stars. Ground-based optical photometry of stars was obtained by Ferraro et al. (1989) and Minniti & Zijlstra (1996, 1997). The presence of a single globular cluster was established, and Hodge et al. (1999) showed that the properties of the globular cluster are similar to those of Galactic globular clusters. In independent Hα imaging programs, Hunter et al. (1993) detected two small shell-like features, and Hodge & Miller (1995) cataloged and measured Hα fluxes for 21 H II regions in the galaxy. Tomita et al. (1998) presented Hα velocity fields for the brightest H II regions in WLM and showed that the southern H II ring is expanding at a speed of 20 km s^{-1} and that the kinetic age of the bubble is 4.5 Myr. Recent studies of the resolved stellar populations with the *Hubble Space Telescope* (*HST*) have been carried out by Dolphin (2000) with the WFPC2 and by Rejkuba et al. (2000) with the Space Telescope Imaging Spectrograph. Dolphin (2000) found that over half of the stars were formed about 9 Gyr ago and that a recent burst of star formation has mostly occurred in the central bar of the galaxy. Rejkuba et al. (2000) identified the horizontal branch, also confirming the presence of a very old stellar population. In the carbon star survey by Battinelli & Demers (2004), they found that WLM contained the largest fraction of carbon to M stars for the dwarf galaxies surveyed and showed that WLM is an inclined disk galaxy with no evidence of an extended spherical stellar halo. Taylor & Klein (2001) searched for molecular gas in WLM, but only upper limits to the CO intensity and subsequent H_2 column densities were determined. Recent 21 cm measurements with the Australia Telescope Compact Array (ATCA) have shown that there are two peaks in the H I distribution and that the measured H I rotation curve is typical for a disk (Jackson et al. 2004).

The spectroscopy of the brightest H II regions was reported by Skillman et al. (1989b) and Hodge & Miller (1995). The resulting nebular oxygen abundances were found to be $12 + \log(\mathrm{O/H}) \simeq 7.74$, or $[\mathrm{O/H}] \simeq -0.92$. Venn et al. (2003) measured the chemical composition of two A-type supergiant stars in WLM and showed that the mean stellar magnesium abundance was $[\mathrm{Mg/H}] = -0.62$. However, the oxygen abundance in one of the stars was $[\mathrm{O/H}] = -0.21$, which is about 0.7 dex,

TABLE 1
Basic Data for WLM

Property	Value	References
Type	IB(s)m	...
Alternate names	DDO 221, UGCA 444	...
Distance	0.95 ± 0.04 Mpc	1
Linear to angular scale at this distance	4.6 pc arcsec^{-1}	2
B_T[a]	11.03 ± 0.08	3
$E(B-V)$[b]	0.037	4
F_{21}[c]	299.8 ± 24.5 Jy km s^{-1}	5
v_{max}[d]	38 ± 5 km s^{-1}	6
[⟨Mg/H⟩][e]	−0.62 ± 0.09 (±0.26)[f]	7
[O/H], WLM 15[g]	−0.21 ± 0.10 (±0.05)[f]	7
[⟨O/H⟩], H II[h]	−0.83 ± 0.06	2

[a] Apparent total B magnitude.
[b] Foreground reddening to the galaxy.
[c] 21 cm flux integral.
[d] Maximum rotation velocity at the last measured point ($r = 0.89$ kpc).
[e] Mean magnesium abundance from supergiants WLM 15 and WLM 31 with the solar value from Grevesse & Sauval (1998).
[f] The first uncertainty represents line-to-line scatter, and the second uncertainty in parentheses is an estimate of the systematic error due to uncertainties in stellar atmospheric parameters (Venn et al. 2003).
[g] Oxygen abundance measured for the supergiant WLM 15 with the solar value from Asplund et al. (2004).
[h] Mean [O III] λ4363 oxygen abundance from H II regions HM 7 and HM 9.
References.—(1) Dolphin 2000; (2) present work; (3) de Vaucouleurs et al. 1991; (4) Schlegel et al. 1998; (5) Barnes & de Blok 2004; (6) Jackson et al. 2004; (7) Venn et al. 2003.

[5] On 1909 October 15, Wolf observed the galaxy for 2 hr with a Waltz reflector at the Heidelberg Observatory atop Königstuhl. He submitted a short description of his observations with the title "Über einen grösseren Nebelfleck in Cetus" (On a Larger Hazy Spot in Cetus) to Astronomische Nachrichten on 1909 November 16.

TABLE 2
PROPERTIES OF EFOSC2 SPECTROGRAPH EMPLOYED AT THE ESO LA SILLA 3.6 m TELESCOPE

Property	Value	
Loral CCD (No. 40)		
Total area (pixel^2)	2048 × 2048	
Field of view (arcmin^2)	5.2 × 5.2	
Pixel size (μm)	15	
Image scale (arcsec pixel^{-1})	0.16	
Gain (e^- ADU^{-1})	1.3	
Read noise (rms) (e^-)	9	
Long Slit		
Length (arcmin)	≃5	
Width (arcsec)	1.5	
	Grating 11	Grating 7
Groove density (lines mm^{-1})	300	600
Blaze λ (first order) (Å)	4000	3800
Dispersion (Å pixel^{-1})	2.04	0.96
Effective λ range (Å)	3380–7520	3270–5240

or almost 5 times larger than the nebular abundance. This presents a vexing question: How can the young supergiant be significantly more metal-rich than the surrounding ISM from which the star was born?

The research reported here is part of a program to understand the chemical evolution from the youngest stellar populations in the nearest dwarf irregular galaxies (e.g., Venn et al. 2001, 2003; Kaufer et al. 2004). The motivations are (1) to obtain a homogeneous sample of abundance measurements for H II regions presently known in WLM; (2) to measure the temperature-sensitive [O III] λ4363 emission line, derive direct oxygen abundances, and compare the present set of measurements with those in the literature; and (3) to examine whether the present measurements show any inhomogeneities in oxygen abundances across the galaxy. This is the first of two papers of our study; the measurements and analyses for H II regions in NGC 6822 will be discussed in the next paper (H. Lee et al. 2005, in preparation). The outline of this paper is as follows. Observations and reductions of the data are presented in § 2. Measurements and analyses are discussed in § 3, and nebular abundances are presented in § 4. Our results are discussed in § 5, and a summary is given in § 6.

2. OBSERVATIONS AND REDUCTIONS

Long-slit spectroscopic observations of H II regions in WLM were carried out on 2003 August 26–28 and 31 (UT) with the ESO Faint Object Spectrograph and Camera (EFOSC2) instrument on the 3.6 m telescope at ESO La Silla Observatory. Details of the instrumentation employed and the log of observations are listed in Tables 2 and 3, respectively. Observing conditions were obtained during the new moon phase. Conditions varied from photometric (August 26 UT) to cloudy (August 31 UT). Two-minute Hα acquisition images were obtained in order to set an optimal position angle of the slit, so that the slit could cover as many H II regions possible. Thirteen H II regions for which spectra were obtained are listed in Table 3 and shown in Figure 1. Identifications for the H II regions follow from the Hα imaging compiled by Hodge & Miller (1995).[6] For completeness, here we provide coordinates (epoch J2000.0) for H II regions that were "newly" resolved in images obtained by the Local Group Survey.[7] HM 16 was resolved into two separate H II regions, which we have called HM 16 NW ($\alpha = 00^h01^m59\overset{s}{.}4$, $\delta = -15°27'24\overset{''}{.}9$), and HM 16 SE ($\alpha = 00^h01^m59\overset{s}{.}6$, $\delta = -15°27'29\overset{''}{.}1$). To the east of H II region HM 18, we took spectra of two additional compact H II regions: HM 18a ($\alpha = 00^h01^m59\overset{s}{.}7$, $\delta = -15°29'30\overset{''}{.}1$) and HM 18b ($\alpha = 00^h01^m59\overset{s}{.}9$, $\delta = -15°29'45\overset{''}{.}5$).

[6] We can also compare the locations of H II regions HM 2, HM 8, and HM 9 in the Hα image by Hodge & Miller (1995) with the [O III] λ5007 image from Jacoby & Lesser (1981).

[7] A description and distribution of the data from the Local Group Survey can be found at http://www.lowell.edu/users/massey/lgsurvey.html (Massey et al. 2002).

TABLE 3
LOG OF OBSERVATIONS

H II Region (1)	Date (UT 2003) (2)	Grating No. (3)	N_{exp} (4)	t_{total} (s) (5)	$\langle X \rangle$ (6)	[O III] λ4363 (7)	rms (mag) (8)
HM 2	Aug 28	11	1 × 1200	1200	1.24	No	0.034
HM 2	Aug 31	7	3 × 1200	3600	1.21	No	0.025
HM 7	Aug 26	11	3 × 1200	3600	1.06	Yes	0.030
HM 8	Aug 26	11	7 × 1200	8400	1.20	No	0.030
HM 9	Aug 26	11	7 × 1200	8400	1.20	Yes	0.030
HM 9	Aug 31	7	3 × 1200	3600	1.21	No	0.025
HM 12	Aug 26	11	3 × 1200	3600	1.06	No	0.030
HM 12	Aug 28	11	3 × 1200	3600	1.08	No	0.034
HM 16 NW	Aug 27	11	3 × 1200	3600	1.04	No	0.029
HM 16 SE	Aug 27	11	3 × 1200	3600	1.04	No	0.029
HM 17	Aug 28	11	3 × 1200	3600	1.03	No	0.034
HM 18	Aug 28	11	3 × 1200	3600	1.03	No	0.034
HM 18a	Aug 28	11	1 × 1200	1200	1.06	No	0.034
HM 18b	Aug 28	11	1 × 1200	1200	1.06	No	0.034
HM 19	Aug 27	11	3 × 1200	3600	1.04	No	0.029
HM 19	Aug 28	11	3 × 1200	3600	1.08	No	0.034
HM 21	Aug 28	11	3 × 1200	3600	1.08	No	0.034

NOTES.—Col. (1): H II region, following the naming convention by Hodge & Miller (1995). Col. (2): Date of observation. Col. (3): Grating. Col. (4): Number of exposures obtained and the length of each exposure in seconds. Col. (5): Total exposure time. Col. (6): Mean effective air mass. Col. (7): [O III] λ4363 detection. Col. (8): Relative rms error in the sensitivity function obtained from observations of standard stars.

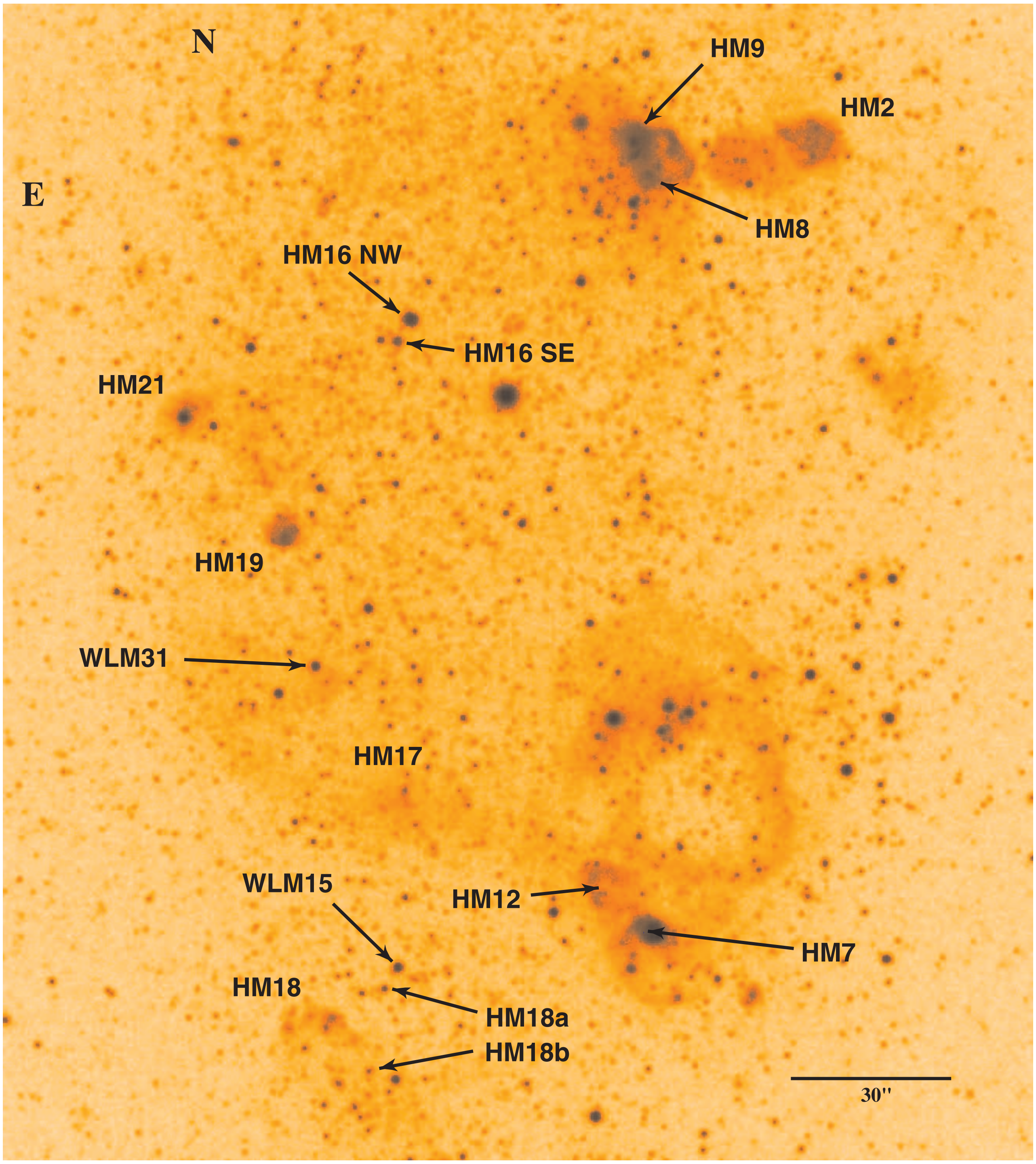

Fig. 1.—Locations in WLM of H ii regions for which spectra were taken. This is an unsubtracted Hα image from the Local Group Survey (Massey et al. 2002). North is up, and east is to the left. Black objects on the image indicate bright sources. The field of view shown is approximately $3'.2 \times 3'.6$. Labels for H ii regions are from Hodge & Miller (1995), except for two compact sources HM 18a and HM 18b. Also marked are two supergiant stars, WLM 15 and WLM 31, for which spectra were measured and analyzed by Venn et al. (2003). The horizontal bar at the bottom right marks an angular scale of 30$''$ on the sky.

Data reductions were carried out in the standard manner using IRAF[8] routines. Data obtained for a given night were reduced independently. The raw two-dimensional images were trimmed, and the bias level was subtracted. Dome flat exposures were used to remove pixel-to-pixel variations in response. Twilight flats were acquired at dusk each night to correct for variations over larger spatial scales. To correct for the "slit function" in the spatial direction, the variation of illumination along the slit was taken into account using dome and twilight flats. Cosmic rays were removed in the addition of multiple exposures for a given H ii region. Wavelength calibration was obtained using helium-argon (He-Ar) arc lamp exposures taken throughout each night. Exposures of standard stars Feige 110, G138-31, LTT 1788, LTT 7379, and LTT 9491 were used for

[8] IRAF is distributed by the National Optical Astronomical Observatory, which is operated by the Associated Universities for Research in Astronomy, Inc., under cooperative agreement with the National Science Foundation.

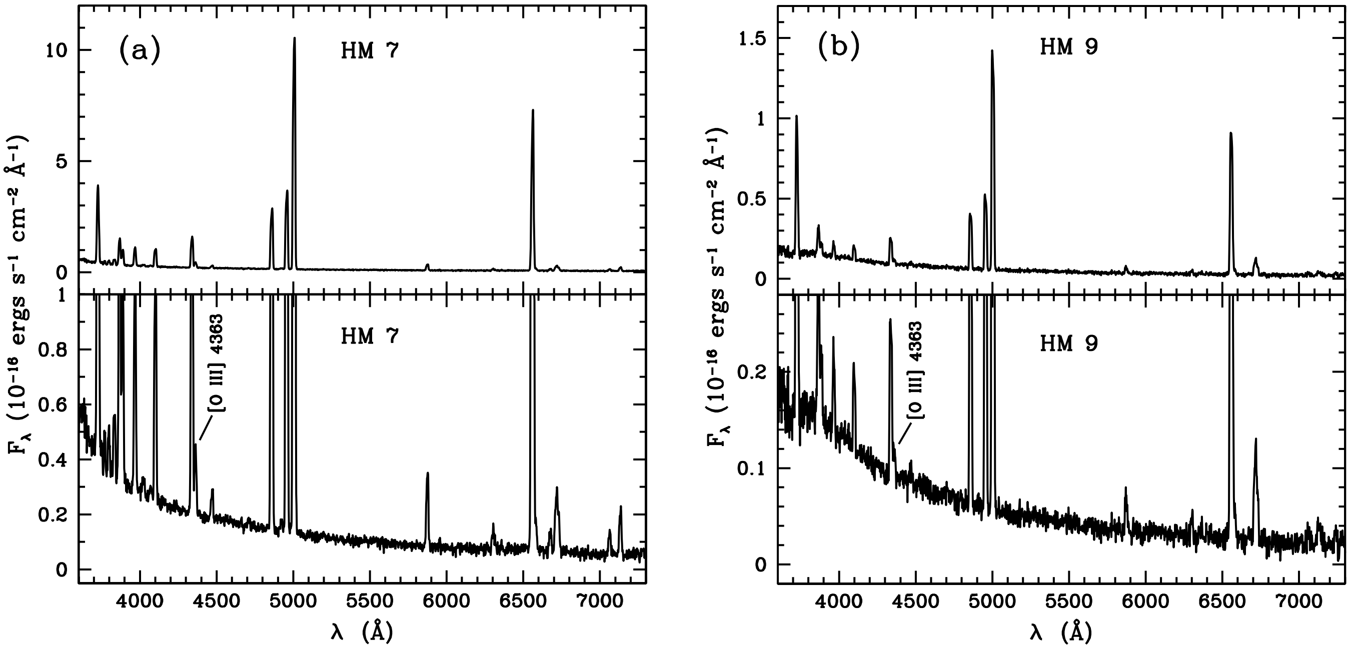

FIG. 2.—Emission-line spectra between 3600 and 7300 Å with grating 11. The observed flux per unit wavelength is plotted vs. wavelength. The bottom panels are expanded to highlight [O III] λ4363. (*a*) H II region HM 7. (*b*) H II region HM 9.

flux calibration. The flux accuracy is listed in Table 3. Final one-dimensional spectra for each H II region were obtained via unweighted summed extractions.

3. MEASUREMENTS AND ANALYSIS

Emission-line strengths were measured using software developed by M. L. McCall and L. Mundy (see Lee 2001; Lee et al. 2003b, 2003c). [O III] λ4363 was detected in H II regions HM 7 and HM 9; these spectra are shown in Figure 2.

Corrections for reddening and for underlying absorption and abundance analyses were performed with SNAP (Spreadsheet Nebular Analysis Package; Krawchuk et al. 1997). Balmer fluxes were first corrected for underlying Balmer absorption with an equivalent width of 2 Å (McCall et al. 1985; Lee et al. 2003c). Hα and Hβ fluxes were used to derive reddening values, $E(B-V)$, using the equation

$$\log\frac{I(\lambda)}{I(\mathrm{H}\beta)} = \log\frac{F(\lambda)}{F(\mathrm{H}\beta)} + 0.4E(B-V)[A_1(\lambda) - A_1(\mathrm{H}\beta)] \tag{1}$$

(Lee et al. 2003b), where F and I are the observed flux and corrected intensity ratios, respectively. Intrinsic case B Balmer line ratios determined by Storey & Hummer (1995) were assumed. The quantity $A_1(\lambda)$ is the extinction in magnitudes for $E(B-V) = 1$; i.e., $A_1(\lambda) = A(\lambda)/E(B-V)$, where $A(\lambda)$ is the monochromatic extinction in magnitudes. Values of A_1 were obtained from the Cardelli et al. (1989) reddening law as defined by a ratio of the total to selective extinction, $R_V = A_V/E(B-V) = 3.07$, which in the limit of zero reddening is the value for an A0 V star (e.g., Vega) with intrinsic color $(B-V)^0 = 0$. Because [S II] $\lambda\lambda$6716, 6731 lines were generally unresolved, $n_e = 100$ cm^{-3} was adopted for the electron density. Errors in the derived $E(B-V)$ were computed from the maximum and minimum values of the reddening based on 2 σ errors in the fits to emission lines.

Observed flux (F) and corrected intensity (I) ratios are listed in Tables 4–7. The listed errors for the observed flux ratios at each wavelength λ account for the errors in the fits to the line profiles, their surrounding continua, and the relative error in the sensitivity function stated in Table 3. Errors in the corrected intensity ratios account for maximum and minimum errors in the flux of the specified line and of the Hβ reference line. At the Hβ reference line, errors for both observed and corrected ratios do not include the error in the flux. Also given for each H II region are the observed Hβ flux, the equivalent width of the Hβ line in emission, and the derived reddening from SNAP.

Where [O III] λ4363 is measured, we also have performed additional computations to check the consistency of our results. Equation (1) can be generalized and rewritten as

$$\log\frac{I(\lambda)}{I(\mathrm{H}\beta)} = \log\frac{F(\lambda)}{F(\mathrm{H}\beta)} + c(\mathrm{H}\beta)f(\lambda), \tag{2}$$

where $c(\mathrm{H}\beta)$ is the logarithmic extinction at Hβ and $f(\lambda)$ is the wavelength-dependent reddening function (Aller 1984; Osterbrock 1989). From equations (1) and (2), we obtain

$$c(\mathrm{H}\beta) = 1.43E(B-V) = 0.47A_V. \tag{3}$$

The reddening function normalized to Hβ is derived from the Cardelli et al. (1989) reddening law, assuming $R_V = 3.07$. As described in Skillman et al. (2003a), values of $c(\mathrm{H}\beta)$ were derived from the error-weighted average of values for the $F(\mathrm{H}\alpha)/F(\mathrm{H}\beta)$, $F(\mathrm{H}\gamma)/F(\mathrm{H}\beta)$, and $F(\mathrm{H}\delta)/F(\mathrm{H}\beta)$ ratios, while simultaneously solving for the effects of underlying Balmer absorption with the equivalent width $\mathrm{EW_{abs}}$. We assumed that $\mathrm{EW_{abs}}$ was the same for Hα, Hβ, Hγ, and Hδ. Uncertainties in $c(\mathrm{H}\beta)$ and $\mathrm{EW_{abs}}$ were determined from Monte Carlo simulations (Olive & Skillman 2001; Skillman et al. 2003a). Errors derived from these simulations are larger than errors quoted in the literature that were either calculated by assuming a constant value for the underlying absorption or derived from a χ^2 analysis in

TABLE 4

Line Ratios and Properties for H II Regions HM 2 and HM 7

Property	$f(\lambda)$	HM 2 (Grating 7) F	HM 2 (Grating 7) I	HM 2 (Grating 11) F	HM 2 (Grating 11) I	HM 7 (Grating 11) F	HM 7 (Grating 11) I
Wavelength (Å):							
[O II] 3727	+0.325	173 ± 13	198 ± 29	139.0 ± 8.9	136 ± 27	116.7 ± 1.9	116.1 ± 1.9
H11 3772	+0.316	...	...	...	...	3.4 ± 1.4	4.2 ± 1.4
H10 3799	+0.310	...	...	...	...	5.3 ± 1.6	6.2 ± 1.5
H9 3835	+0.302	...	...	...	...	7.65 ± 0.91	8.77 ± 0.91
[Ne III] 3869	+0.294	55.3 ± 7.6	60 ± 13	48.8 ± 5.2	48 ± 11	39.25 ± 0.95	39.06 ± 0.95
H8 + He I 3889	+0.289	...	...	...	...	22.33 ± 0.87	23.54 ± 0.87
Hϵ + He I 3970[a]	+0.269	36.1 ± 5.6	42 ± 10	21.2 ± 4.4	25.2 ± 9.5	27.84 ± 0.66	28.92 ± 0.66
He I 4027	+0.253	...	...	...	...	1.96 ± 0.48	1.95 ± 0.48
[S II] 4068	+0.241	...	...	...	...	1.00 ± 0.59	1.00 ± 0.59
Hδ 4101	+0.232	38.1 ± 6.1	43 ± 11	18.4 ± 2.5	21.6 ± 6.2	27.49 ± 0.77	28.43 ± 0.77
Hγ 4340	+0.158	42.9 ± 5.3	46.8 ± 9.6	48.6 ± 3.7	51 ± 11	47.2 ± 1.0	47.8 ± 1.0
[O III] 4363	+0.151	...	...	<12.3	<12.0	7.95 ± 0.80	7.91 ± 0.80
He I 4388	+0.143	...	...	...	...	0.63 ± 0.81	0.63 ± 0.81
He I 4471	+0.116	...	...	...	...	3.56 ± 0.25	3.54 ± 0.25
[Ar IV] + He I 4713	+0.042	...	...	...	...	0.98 ± 0.17	0.98 ± 0.17
[Ar IV] 4740	+0.034	...	...	...	...	0.34 ± 0.14	0.34 ± 0.14
Hβ 4861	0.000	100.0 ± 5.7	100.0 ± 6.8	100 ± 11	100 ± 12	100.0 ± 3.7	100.0 ± 3.6
[O III] 4959	−0.026	187.9 ± 5.3	183 ± 20	213 ± 12	209 ± 39	133.9 ± 9.1	133.2 ± 9.1
[O III] 5007	−0.038	529.7 ± 6.4	516 ± 52	568 ± 15	556 ± 92	390 ± 12	388 ± 12
He I 5876	−0.204	...	...	...	...	10.45 ± 0.38	10.40 ± 0.38
[O I] 6300	−0.264	...	...	...	...	2.89 ± 0.31[b]	2.88 ± 0.31
[O I] 6363	−0.272	...	...	...	...	0.52 ± 0.24	0.51 ± 0.24
Hα 6563	−0.299	...	...	280.0 ± 8.7	276 ± 47	270.5 ± 7.2	269.4 ± 7.2
[N II] 6583	−0.301	...	...	...	...	4.84 ± 0.59	4.81 ± 0.59
He I 6678	−0.314	...	...	...	...	3.11 ± 0.30	3.09 ± 0.30
[S II] 6716	−0.319	...	...	...	...	7.57 ± 0.44	7.53 ± 0.44
[S II] 6731	−0.321	...	...	...	...	4.91 ± 0.38	4.89 ± 0.38
He I 7065	−0.366	...	...	...	...	2.95 ± 0.21	2.94 ± 0.21
[Ar III] 7136	−0.375	...	...	...	...	5.87 ± 0.23	5.84 ± 0.23
[O II] 7320	−0.400	...	...	...	...	1.51 ± 0.22	1.50 ± 0.22
[O II] 7330	−0.401	...	...	...	...	1.84 ± 0.23	1.83 ± 0.23
F(Hβ) (ergs s^{-1} cm^{-2})		(4.54 ± 0.26) × 10^{-16}		(2.47 ± 0.27) × 10^{-15}		(4.63 ± 0.17) × 10^{-15}	
EW$_e$(Hβ) (Å)		121 ± 20		98 ± 22		403 ± 114	
Derived $E(B-V)$ (mag)[c]		+0.087 ± 0.395		−0.038 ± 0.165		−0.061 ± 0.049	
c(Hβ)		...		...		0	
Adopted A_V (mag)		+0.28		0		0	
EW$_{abs}$ (Å)		2		2		2	

Notes.—F is the observed flux ratio with respect to Hβ. I is the corrected intensity ratio, corrected for the adopted reddening listed and for underlying Balmer absorption. The uncertainties in the observed line ratios account for the uncertainties in the fits to the line profiles, the surrounding continua, and the relative uncertainty in the sensitivity function listed in Table 3. Flux uncertainties in the Hβ reference line are not included. Uncertainties in the corrected line ratios account for uncertainties in the specified line and in the Hβ reference line. The reddening function, f(λ), from eq. (2) is given. Also listed are the observed Hβ flux; the equivalent width of Hβ in emission, EW$_e$(Hβ); and derived values of the reddenings from SNAP using eq. (1). Where [O III] λ4363 is measured, simultaneous solutions for the logarithmic reddening, c(Hβ), from eq. (2) and the equivalent width of the underlying Balmer absorption, EW$_{abs}$, are listed. The adopted value of the extinction in V, A_V, is listed. Where [O III] λ4363 is not measured, the equivalent width of the underlying Balmer absorption was set to 2 Å.

[a] Blended with [Ne III] λ3967.

[b] Blended with [S III] λ6312.

[c] HM 2 (gr 7): derived from F(Hγ)/F(Hβ); HM 2 and HM 7 (gr 11): derived from F(Hα)/F(Hβ).

the absence of Monte Carlo simulations for the errors; Figure 3 shows an example of these simulations for H II region HM 9. In Tables 4, 5, and 6, we included the logarithmic reddening and the equivalent width of the underlying Balmer absorption, which were solved simultaneously. Values for the logarithmic reddening are consistent with values of the reddening determined with SNAP. Where negative values were derived, the reddening was set to zero in correcting line ratios and in abundance calculations.

4. NEBULAR ABUNDANCES

Oxygen abundances in H II regions were derived using three methods: (1) the direct method (e.g., Dinerstein 1990; Skillman 1998; Garnett 2004) and (2) and (3) two bright-line methods discussed by McGaugh (1991; based on photoionization models) and Pilyugin (2000; purely empirical), respectively.

4.1. *Oxygen Abundances:* [O III] λ4363 *Temperatures*

For the "direct" conversion of emission-line intensities into ionic abundances, a reliable estimate of the electron temperature in the ionized gas is required. To describe the ionization structure of H II regions, we adopt a two-zone model, with a low- and a high-ionization zone characterized by temperatures $T_e(O^+)$ and $T_e(O^{+2})$, respectively. The temperature in the O^{+2} zone is measured with the emission-line ratio I([O III] λ5007)/I([O III]

TABLE 5

Line Ratios and Properties for H ii Region HM 9

Property	$f(\lambda)$	HM 9 Aperture 1 (Grating 7) F	HM 9 Aperture 1 (Grating 7) I	HM 9 Aperture 2[a] (Grating 7) F	HM 9 Aperture 2[a] (Grating 7) I	HM 9 Aperture 3 (Grating 7) F	HM 9 Aperture 3 (Grating 7) I
Wavelength (Å):							
[O ii] 3727	+0.325	264.5 ± 6.2	261 ± 20	301.6 ± 6.7	296 ± 22	407 ± 16	397 ± 47
[Ne iii] 3869	+0.294	34.8 ± 3.7	34.3 ± 5.1	34.0 ± 4.4	33.4 ± 5.7	46 ± 11	45 ± 14
Hϵ + He i 3970	+0.269	23.8 ± 2.5	26.6 ± 4.3	23.1 ± 2.5	26.4 ± 4.4	44.6 ± 8.1	48 ± 13
Hδ 4101	+0.232	25.1 ± 2.2	27.8 ± 4.0	24.5 ± 2.2	27.5 ± 4.0	26.5 ± 6.5	30 ± 11
Hγ 4340	+0.158	45.7 ± 2.3	47.4 ± 4.8	47.8 ± 2.5	49.5 ± 5.0	54.7 ± 6.9	56 ± 12
[O iii] 4363	+0.151	<7.3	<7.2	<8.3	<8.1	...	...
Hβ 4861	0.000	100.0 ± 2.2	100.0 ± 3.8	100.0 ± 2.2	100.0 ± 3.8	100.0 ± 5.8	100.0 ± 6.9
[O iii] 4959	−0.026	102.6 ± 2.9	101.1 ± 8.0	93.9 ± 2.7	92.3 ± 7.4	70.7 ± 5.3	69 ± 10
[O iii] 5007	−0.038	305.0 ± 3.5	300 ± 21	279.5 ± 3.3	275 ± 19	203.1 ± 6.4	198 ± 22
F(Hβ) (ergs s^{-1} cm^{-2})		$(9.70 \pm 0.21) \times 10^{-16}$		$(1.608 \pm 0.036) \times 10^{-15}$		$(2.87 \pm 0.17) \times 10^{-16}$	
EW$_e$(Hβ) (Å)		132.5 ± 9.4		114.3 ± 7.2		80 ± 10	
Derived $E(B-V)$ (mag)[b]		−0.025 ± 0.195		−0.108 ± 0.197		−0.338 ± 0.409	
c(Hβ)		...		...		...	
Adopted A_V (mag)		0		0		0	
EW$_{abs}$ (Å)		2		2		2	

Property	$f(\lambda)$	HM 9 Aperture 1 (Grating 11) F	HM 9 Aperture 1 (Grating 11) I	HM 9 Aperture 2[a] (Grating 11) F	HM 9 Aperture 2[a] (Grating 11) I	HM 9 Aperture 3 (Grating 11) F	HM 9 Aperture 3 (Grating 11) I
Wavelength (Å):							
[O ii] 3727	+0.325	208.7 ± 4.2	202 ± 11	215.9 ± 4.2	209 ± 12	213.4 ± 4.8	204 ± 12
[Ne iii] 3869	+0.294	40.4 ± 1.7	39.1 ± 2.5	42.7 ± 1.2	41.3 ± 2.3	48.0 ± 2.3	45.9 ± 3.1
H8 + He i 3889	+0.289	15.7 ± 1.4	23.0 ± 1.7	16.5 ± 1.0	24.3 ± 1.5	13.2 ± 1.8	24.5 ± 2.1
Hϵ + He i 3970	+0.269	22.7 ± 1.5	29.1 ± 1.9	20.1 ± 1.1	27.2 ± 1.6	17.0 ± 2.0	27.4 ± 2.3
Hδ 4101	+0.232	20.4 ± 1.5	26.3 ± 1.8	19.9 ± 1.1	26.1 ± 1.4	16.8 ± 1.6	25.8 ± 1.8
Hγ 4340	+0.158	45.6 ± 1.5	49.1 ± 1.9	45.3 ± 1.4	48.9 ± 1.8	43.5 ± 2.2	48.6 ± 2.5
[O iii] 4363	+0.151	7.1 ± 1.1	6.9 ± 1.1	6.5 ± 1.1	6.3 ± 1.1	5.7 ± 1.7	5.4 ± 1.6
He i 4471	+0.116	...	...	3.36 ± 0.67	3.25 ± 0.65	3.67 ± 0.90	3.50 ± 0.86
Hβ 4861	0.000	100.0 ± 3.9	100.0 ± 3.8	100.0 ± 3.8	100.0 ± 3.7	100.0 ± 4.2	100.0 ± 4.0
[O iii] 4959	−0.026	143 ± 11	138 ± 11	140 ± 11	135 ± 11	135.1 ± 9.7	128.9 ± 9.3
[O iii] 5007	−0.038	420 ± 14	406 ± 14	407 ± 14	394 ± 14	392 ± 12	374 ± 12
He i 5876	−0.204	10.6 ± 1.1	10.3 ± 1.1	10.39 ± 0.78	10.05 ± 0.82	10.9 ± 1.5	10.4 ± 1.5
Hα 6563	−0.299	279.9 ± 8.7	272 ± 16	287.3 ± 9.4	279 ± 16	295.0 ± 9.2	282 ± 16
[N ii] 6583	−0.301	<4.6	<4.5	7.7 ± 2.3	7.5 ± 2.3	8.7 ± 1.8	8.3 ± 1.8
[S ii] 6716, 6731	−0.320	29.8 ± 1.8	28.8 ± 2.3	35.2 ± 1.7	34.0 ± 2.4	41.9 ± 2.6	39.9 ± 3.2
[Ar iii] 7136	−0.375	8.7 ± 1.1	8.6 ± 1.6	8.00 ± 0.89	7.9 ± 1.3	8.9 ± 2.4	8.7 ± 2.8
F(Hβ) (ergs s^{-1} cm^{-2})		$(2.67 \pm 0.11) \times 10^{-16}$		$(6.52 \pm 0.25) \times 10^{-16}$		$(1.942 \pm 0.082) \times 10^{-16}$	
EW$_e$(Hβ) (Å)		123 ± 11		111.0 ± 8.7		84.4 ± 6.1	
Derived $E(B-V)$ (mag)[c]		−0.036 ± 0.096		−0.012 ± 0.096		+0.009 ± 0.099	
c(Hβ)		−0.04 ± 0.07		−0.01 ± 0.07		+0.00 ± 0.07	
Adopted A_V (mag)		0		0		0	
EW$_{abs}$ (Å)		4.1 ± 2.0		3.8 ± 1.4		4.1 ± 1.3	

Notes.—Grating 7: long slit aligned with HM 2. Grating 11: long slit aligned with HM 8. Thus, spectra for the first aperture in both grating settings are likely at the same position within the HM 9 nebula. F is the observed flux ratio with respect to Hβ. I is the corrected intensity ratio, corrected for the adopted reddening listed and for underlying Balmer absorption. The uncertainties in the observed line ratios account for the uncertainties in the fits to the line profiles, the surrounding continua, and the relative uncertainty in the sensitivity function listed in Table 3. Flux uncertainties in the Hβ reference line are not included. Uncertainties in the corrected line ratios account for uncertainties in the specified line and in the Hβ reference line. The reddening function, f(λ), from eq. (2) is given. Also listed are the observed Hβ flux; the equivalent width of Hβ in emission, EW$_e$(Hβ); and derived values of the reddenings from SNAP using eq. (1). Where [O iii] λ4363 is measured, simultaneous solutions for the logarithmic reddening, c(Hβ), from eq. (2) and the equivalent width of the underlying Balmer absorption, EW$_{abs}$, are listed. The adopted value of the extinction in V, A_V, is listed. Where [O iii] λ4363 is not measured, the equivalent width of the underlying Balmer absorption was set to 2 Å.

[a] For the given grating setting, the definition for aperture 2 encompasses regions 1 and 3.

[b] Derived from $F(\mathrm{H}\gamma)/F(\mathrm{H}\beta)$ ratios.

[c] Derived from $F(\mathrm{H}\alpha)/F(\mathrm{H}\beta)$ ratios.

λ4363) (Osterbrock 1989). The temperature in the O$^+$ zone is given by

$$t_e([\mathrm{O\ II}]) = 0.7 t_e([\mathrm{O\ III}]) + 0.3, \quad (4)$$

where $t_e = T_e/10^4$ K (Campbell et al. 1986; Garnett 1992). The uncertainty in T_e(O^{+2}) is computed from the maximum and minimum values derived from the uncertainties in corrected emission-line ratios. The computation does not include uncertainties in the reddening (if any), the uncertainties in the atomic data, or the presence of temperature fluctuations. The uncertainty in T_e(O$^+$) is assumed to be the same as the uncertainty in T_e(O^{+2}). These temperature uncertainties are conservative estimates and are likely overestimates of the actual

TABLE 6
Line Ratios and Properties for H II Regions HM 8, 12, 16, and 17

Property	$f(\lambda)$	HM 8 (Grating 11)		HM 12 (Grating 11)[a]		HM 12 (Grating 11)[b]	
		F	I	F	I	F	I
Wavelength (Å):							
[O II] 3727	+0.325	350 ± 15	339 ± 43	445 ± 12	432 ± 42	289.9 ± 9.9	281 ± 34
[Ne III] 3869	+0.294	...	...	...	...	37.1 ± 5.7	36.0 ± 8.3
Hδ 4101	+0.232	...	...	...	...	22.2 ± 6.0	25 ± 10
Hγ 4340	+0.158	39.7 ± 4.9	40.7 ± 8.6	33.6 ± 3.3	36.9 ± 6.3	49.2 ± 5.6	51 ± 10
Hβ 4861	0.000	100.0 ± 6.5	100.0 ± 7.5	100.0 ± 4.5	100.0 ± 5.6	100.0 ± 6.1	100.0 ± 7.3
[O III] 4959	−0.026	46.9 ± 5.6	45.4 ± 9.0	40.1 ± 4.0	38.9 ± 6.2	75.6 ± 6.0	73 ± 12
[O III] 5007	−0.038	144.1 ± 7.0	140 ± 18	114.8 ± 4.8	111 ± 12	257.0 ± 8.0	249 ± 30
He I 5876	−0.204	...	...	...	...	15.0 ± 3.3	14.6 ± 4.4
Hα 6563	−0.299	266 ± 10	264 ± 33	284 ± 10	277 ± 29	288.5 ± 9.1	282 ± 34
[N II] 6583	−0.301	...	...	<7.7	<7.5	...	...
[S II] 6716, 6731	−0.320	29.6 ± 5.1	28.7 ± 7.2	69.2 ± 7.2	67 ± 11	37.0 ± 4.6	36.0 ± 7.3
F(Hβ) (ergs s^{-1} cm^{-2})		$(4.50 \pm 0.29) \times 10^{-17}$		$(1.85 \pm 0.08) \times 10^{-16}$		$(3.43 \pm 0.21) \times 10^{-16}$	
EW$_e$(Hβ) (Å)		62.2 ± 5.8		64.9 ± 4.3		66.5 ± 6.2	
Derived $E(B-V)$ (mag)		−0.083 ± 0.124		−0.035 ± 0.106		−0.016 ± 0.121	
c(Hβ)		...		...		...	
Adopted A_V (mag)		0		0		0	
EW$_{abs}$ (Å)		2		2		2	

Property	$f(\lambda)$	HM 16 NW (Grating 11)		HM 16 SE (Grating 11)		HM 17 (Grating 11)	
		F	I	F	I	F	I
Wavelength (Å):							
[O II] 3727	+0.325	309.0 ± 6.0	431 ± 33	470 ± 19	700 ± 94	448 ± 16	428 ± 55
Hϵ + He I 3970	+0.269	13.2 ± 1.5	19.9 ± 3.6	...	...	...	...
Hδ 4101	+0.232	17.1 ± 1.5	23.4 ± 3.4	...	...	...	...
Hγ 4340	+0.158	41.8 ± 1.6	48.9 ± 4.5	46.5 ± 7.6	60 ± 17	35.7 ± 6.1	39 ± 11
[O III] 4363	+0.151	<4.8	<5.3	...	...	...	...
Hβ 4861	0.000	100.0 ± 2.8	100.0 ± 4.1	100.0 ± 7.2	100.0 ± 8.3	100.0 ± 6.7	100.0 ± 7.9
[O III] 4959	−0.026	71.1 ± 4.6	68.8 ± 7.7	10.8 ± 5.5	9.9 ± 5.9	...	...
[O III] 5007	−0.038	214.2 ± 6.0	205 ± 17	13.2 ± 5.6	12.0 ± 6.2	56.6 ± 5.2	54.0 ± 9.6
He I 5876	−0.204	10.6 ± 1.6	8.8 ± 1.7	...	...	...	...
Hα 6563	−0.299	370.5 ± 8.3	286 ± 23	416 ± 13	286 ± 36	256.6 ± 9.8	248 ± 33
[N II] 6583	−0.301	14.2 ± 3.2	10.9 ± 3.0	...	...	...	...
[S II] 6716, 6731	−0.320	26.5 ± 3.2	20.1 ± 3.3	64.8 ± 9.2	43.3 ± 9.9	42.6 ± 5.7	40.6 ± 8.9
F(Hβ) (ergs s^{-1} cm^{-2})		$(6.86 \pm 0.19) \times 10^{-16}$		$(1.38 \pm 0.10) \times 10^{-16}$		$(2.39 \pm 0.16) \times 10^{-16}$	
EW$_e$(Hβ) (Å)		156 ± 13		34.6 ± 2.9		41.7 ± 3.3	
Derived $E(B-V)$ (mag)		+0.251 ± 0.080		+0.332 ± 0.128		−0.145 ± 0.133	
c(Hβ)		...		...		2...	
Adopted A_V (mag)		+0.77		+1.0		0	
EW$_{abs}$ (Å)		2		2		2	

Notes.—F is the observed flux ratio with respect to Hβ. I is the corrected intensity ratio, corrected for the adopted reddening listed and for underlying Balmer absorption. The uncertainties in the observed line ratios account for the uncertainties in the fits to the line profiles, the surrounding continua, and the relative uncertainty in the sensitivity function listed in Table 3. Flux uncertainties in the Hβ reference line are not included. Uncertainties in the corrected line ratios account for uncertainties in the specified line and in the Hβ reference line. The reddening function, f(λ), from eq. (2) is given. Also listed are the observed Hβ flux; the equivalent width of Hβ in emission, EW$_e$(Hβ); and derived values of the reddenings from SNAP using eq. (1). Where [O III] λ4363 is measured, simultaneous solutions for the logarithmic reddening, c(Hβ), from eq. (2) and the equivalent width of the underlying Balmer absorption, EW$_{abs}$, are listed. The adopted value of the extinction in V, A_V, is listed. Where [O III] λ4363 is not measured, the equivalent width of the underlying Balmer absorption was set to 2 Å.

[a] Observed August 26 (UT); long slit aligned with HM 7.

[b] Observed August 28 (UT); long slit aligned with HM 19 and HM 21.

uncertainties. For subsequent calculations of ionic abundances, we assume the following electron temperatures for specific ions (Garnett 1992): $t_e(\mathrm{N}^+) = t_e(\mathrm{O}^+)$, $t_e(\mathrm{Ne}^{+2}) = t_e(\mathrm{O}^{+2})$, $t_e(\mathrm{Ar}^{+2}) = 0.83 t_e(\mathrm{O}^{+2}) + 0.17$, and $t_e(\mathrm{Ar}^{+3}) = t_e(\mathrm{O}^{+2})$.

The total oxygen abundance by number is given by $\mathrm{O/H} = \mathrm{O}^0/\mathrm{H} + \mathrm{O}^+/\mathrm{H} + \mathrm{O}^{+2}/\mathrm{H} + \mathrm{O}^{+3}/\mathrm{H}$. For conditions found in typical H II regions and those presented here, very little oxygen in the form of O^0 is expected, and it is not included here. In the absence of He II emission, the O^{+3} contribution is considered to be negligible. Ionic abundances for O^+/H and O^{+2}/H were computed using O^+ and O^{+2} temperatures, respectively, as described above.

Measurements of the [O III] λ4363 line were obtained, and subsequent electron temperatures were derived in HM 7 and HM 9. Ionic abundances and total abundances are computed using the method described by Lee et al. (2003b). With SNAP, oxygen abundances were derived using the five-level atom approximation (DeRobertis et al. 1987) and transition probabilities and collision strengths for oxygen from Pradhan (1976), McLaughlin & Bell (1993), Lennon & Burke (1994), and Wiese

TABLE 7

Line Ratios and Properties for H II Regions HM 18, 18a, 18b, 19, and 21

Property	$f(\lambda)$	HM 18 (Grating 11)[a] F	HM 18 (Grating 11)[a] I	HM 18a (Grating 11)[b] F	HM 18a (Grating 11)[b] I	HM 18b (Grating 11) F	HM 18b (Grating 11) I
Wavelength (Å):							
[O II] 3727	+0.325	790 ± 41	1000 ± 200	...	...		
Hβ 4861	0.000	100 ± 10	100 ± 14	100 ± 19		100 ± 17	
Hα 6563	−0.299	618 ± 18	286 ± 54	554 ± 37		881 ± 50	
[S II] 6716, 6731	−0.320	92 ± 14	40 ± 12	...	...		
F(Hβ) (ergs s^{-1} cm^{-2})		(9.50 ± 0.99) × 10^{-17}		(1.47 ± .27) × 10^{-16}		(7.6 ± 1.3) × 10^{-17}	
EW$_e$(Hβ) (Å)		4.61 ± 0.48		8.8 ± 1.6		10.7 ± 1.9	
Derived $E(B-V)$ (mag)		+0.445 ± 0.190		+0.481 ± 0.308		+0.982 ± 0.277	
c(Hβ)		...		...		...	
Adopted A_V (mag)		+1.37		+1.48		+3.01	
EW$_{abs}$ (Å)		2		2		2	

Property	$f(\lambda)$	HM 19 (Grating 11)[a] F	HM 19 (Grating 11)[a] I	HM 19 (Grating 11)[b] F	HM 19 (Grating 11)[b] I	HM 21 (Grating 11) F	HM 21 (Grating 11) I
Wavelength (Å):							
[O II] 3727	+0.325	350.2 ± 9.0	467 ± 48	131.6 ± 4.6	184 ± 16	387.0 ± 7.9	404 ± 38
[Ne III] 3869	+0.294	...	...	17.1 ± 3.0	22.4 ± 4.9	...	...
Hε + He I 3970	+0.269	...	...	...	...	12.9 ± 2.4	18.5 ± 5.7
Hδ 4101	+0.232	...	...	10.6 ± 1.6	24.0 ± 6.6	20.9 ± 2.2	26.1 ± 4.8
Hγ 4340	+0.158	39.2 ± 3.3	46.7 ± 7.5	30.0 ± 1.5	41.7 ± 4.7	43.6 ± 2.0	47.3 ± 5.5
Hβ 4861	0.000	100.0 ± 5.4	100.0 ± 6.3	100.0 ± 1.9	100.0 ± 4.0	100.0 ± 4.0	100.0 ± 5.4
[O III] 4959	−0.026	67.6 ± 5.0	65.0 ± 9.3	10.7 ± 1.4	9.9 ± 1.8	56.9 ± 3.8	55.2 ± 7.1
[O III] 5007	−0.038	177.7 ± 6.1	170 ± 18	36.4 ± 1.6	33.3 ± 3.2	175.7 ± 4.9	170 ± 17
Hα 6563	−0.299	363 ± 14	286 ± 32	397.1 ± 4.0	286 ± 22	308.1 ± 7.6	286 ± 28
[N II] 6583	−0.301	...	...	6.7 ± 3.3	4.8 ± 2.6	<13	<12
[S II] 6716, 6731	−0.320	...	...	8.4 ± 1.3	5.9 ± 1.1	35.3 ± 3.9	32.6 ± 5.6
F(Hβ) (ergs s^{-1} cm^{-2})		(3.78 ± 0.20) × 10^{-16}		(9.24 ± 0.17) × 10^{-16}		(6.70 ± 0.27) × 10^{-16}	
EW$_e$(Hβ) (Å)		100 ± 11		35.54 ± 0.75		71.8 ± 4.6	
Derived $E(B-V)$ (mag)		+0.223 ± 0.113		+0.285 ± 0.077		+0.050 ± 0.098	
c(Hβ)		...		...		...	
Adopted A_V (mag)		+0.68		+0.87		+0.15	
EW$_{abs}$ (Å)		2		2		2	

Notes.—F is the observed flux ratio with respect to Hβ. I is the corrected intensity ratio, corrected for the adopted reddening listed and for underlying Balmer absorption. The uncertainties in the observed line ratios account for the uncertainties in the fits to the line profiles, the surrounding continua, and the relative uncertainty in the sensitivity function listed in Table 3. Flux uncertainties in the Hβ reference line are not included. Uncertainties in the corrected line ratios account for uncertainties in the specified line and in the Hβ reference line. The reddening function, f(λ), from eq. (2) is given. Also listed are the observed Hβ flux; the equivalent width of Hβ in emission, EW$_e$(Hβ); and derived values of the reddenings from SNAP using eq. (1). Where [O III] λ4363 is measured, simultaneous solutions for the logarithmic reddening, c(Hβ), from eq. (2) and the equivalent width of the underlying Balmer absorption, EW$_{abs}$, are listed. The adopted value of the extinction in V, A_V, is listed. Where [O III] λ4363 is not measured, the equivalent width of the underlying Balmer absorption was set to 2 Å.

[a] Observed August 27 (UT); long slit aligned with HM 16 NW and HM 16 SE.

[b] Observed August 28 (UT); long slit aligned with HM 21.

et al. (1996); Balmer line emissivities from Storey & Hummer (1995) were used. Derived ionic and total abundances are listed in Tables 8 and 9. These tables include derived O^+ and O^{+2} electron temperatures, O^+ and O^{+2} ionic abundances, and the total oxygen abundances. Errors in direct oxygen abundances computed with SNAP have two contributions: the maximum and minimum values for abundances from errors in the temperature, and the maximum and minimum possible values for the abundances from propagated errors in the intensity ratios. These uncertainties in oxygen abundances are also conservative estimates.

Using the method described by Skillman et al. (2003a), we recompute oxygen abundances in H II regions with [O III] λ4363 detections. Abundances are computed using the emissivities from the five-level atom program by Shaw & Dufour (1995). As described above, we use the same two-temperature zone model and temperatures for the remaining ions. The error in $T_e(O^{+2})$ is derived from the uncertainties in the corrected emission-line ratios and does not include any uncertainties in the atomic data, or the possibility of temperature variations within the O^{+2} zone. The fractional error in $T_e(O^{+2})$ is applied similarly to $T_e(O^+)$ to compute the uncertainty in the latter. Uncertainties in the resulting ionic abundances are combined in quadrature for the final uncertainty in the total linear (summed) abundance. The adopted [O III] λ4363 abundances and their uncertainties computed in this manner are listed in Tables 8 and 9. Direct oxygen abundances computed with SNAP are in excellent agreement with direct oxygen abundances computed with the method described by Skillman et al. (2003a); abundances from the two methods agree to within 0.02 dex.

Direct oxygen abundances for H II regions HM 7 and HM 9 are $12 + \log(O/H) = 7.72 \pm 0.04$ and 7.91 ± 0.04, respectively; the latter is a weighted mean of the three measured values shown in Table 9. The mean oxygen abundance for these

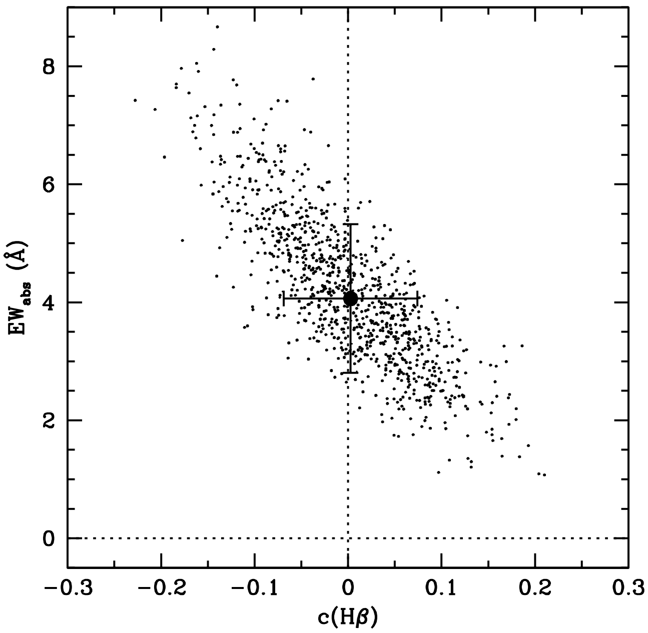

FIG. 3.—Monte Carlo simulations of solutions for the reddening, $c(\mathrm{H}\beta)$, and the underlying Balmer absorption with equivalent width, $\mathrm{EW_{abs}}$, from hydrogen Balmer flux ratios. Dotted lines mark zero values for each quantity. The results here are shown for the H II region HM 9. Each small point is a solution derived from a different realization of the same input spectrum. The large filled circle with error bars shows the mean result with 1 σ errors derived from the dispersion in the solutions.

two H II regions is $(\mathrm{O/H}) = (6.69 \pm 0.93) \times 10^{-5}$, or $12 + \log(\mathrm{O/H}) = 7.83 \pm 0.06$. This value corresponds to $[\mathrm{O/H}] = -0.83$, or 15% of the solar value. For historical completeness, we note that our derived nebular oxygen abundance would correspond to $[\mathrm{O/H}] = -1.10$ for the Anders & Grevesse (1989) value of the solar oxygen abundance.

4.2. *Oxygen Abundances: Bright-Line Methods*

For H II regions without [O III] $\lambda 4363$ measurements, secondary methods are necessary to derive oxygen abundances. The bright-line method is so called because the oxygen abundance is given in terms of the bright [O II] and [O III] lines. Pagel et al. (1979) suggested using

$$R_{23} = I([\mathrm{O\,II}]\lambda 3727) + I([\mathrm{O\,III}]\lambda 4959) I(\mathrm{H}\beta) \tag{5}$$

as an abundance indicator. Using photoionization models, Skillman (1989) showed that bright [O II] and [O III] line intensities can be combined to determine uniquely the ionization parameter and an "empirical" oxygen abundance in low-metallicity H II regions. McGaugh (1991) developed a grid of photoionization models and suggested using R_{23} and $O_{32} = I([\mathrm{O\,III}]\lambda\lambda 4959, 5007)/I([\mathrm{O\,II}]\lambda 3727)$ to estimate the oxygen abundance.[9] However, the calibration is degenerate such that for a given value of R_{23}, two values of the oxygen abundance are possible. The [N II]/[O II] ratio was suggested (e.g., McCall et al. 1985; McGaugh 1994; van Zee et al. 1998) as the discriminant to choose between the "upper branch" (high oxygen abundance) or the "lower branch" (low oxygen abundance). In the present set of spectra, [N II] line strengths are generally small, and [N II]/[O II] has been found to be less than the threshold value of 0.1. Pilyugin (2000) proposed a new calibration of the oxygen abundances using bright oxygen lines. At low abundances [$12 + \log(\mathrm{O/H}) \lesssim 8.2$], his calibration is expressed as

$$12 + \log(\mathrm{O/H}) = 6.35 + 3.19 \log R_{23} - 1.74 \log R_3, \tag{6}$$

where R_{23} is given by equation (5) and $R_3 = I([\mathrm{O\,III}]\lambda\lambda 4959, 5007)/I(\mathrm{H}\beta)$. In some instances, oxygen abundances with the McGaugh method could not be computed because the R_{23} values were outside of the effective range for the models. Skillman et al. (2003a) have shown that the Pilyugin calibration covers the highest values of R_{23}.

Oxygen abundances derived using the McGaugh and Pilyugin bright-line calibrations are listed in Tables 8 and 9. For each H II region, differences between direct and bright-line abundances are shown as a function of O_{32} and R_{23} in Figure 4. The difference between the McGaugh and Pilyugin calibrations (indicated by asterisks) appears to correlate with $\log O_{32}$, which has been previously noticed by Skillman et al. (2003a), Lee et al. (2003a), and Lee & Skillman (2004). Despite the small number of [O III] $\lambda 4363$ detections, we find that bright-line abundances with the McGaugh and the Pilyugin calibrations are $\approx$0.10–0.15 dex larger and $\approx$0.05–0.10 dex smaller, respectively, than the corresponding direct abundances. We note also that H II region HM 19 exhibits the lowest values of R_{23} and O_{32} ($\log R_{23} = 0.357$, $\log O_{32} = -0.629$) and is the outlier in the lower left corner of both panels in Figure 4. Generally, in the absence of [O III] $\lambda 4363$, an estimate of the oxygen abundance from the bright-line calibration is good to within $\approx$0.2 dex.

4.3. *Element Ratios*

We consider next argon-to-oxygen, nitrogen-to-oxygen, and neon-to-oxygen ratios, which are listed in Tables 8 and 9. For metal-poor galaxies, it is assumed that $\mathrm{N/O} \approx \mathrm{N^+/O^+}$ (Garnett 1990), and $\mathrm{N^+/O^+}$ values were derived. Nitrogen abundances were computed as $\mathrm{N/H} = \mathrm{ICF(N)(N^+/H)}$. The ionization correction factor, $\mathrm{ICF(N)} = \mathrm{O/O^+}$, accounts for missing ions. The resulting nitrogen-to-oxygen abundance ratios were found to be the same as the $\mathrm{N^+/O^+}$ values. The mean value of $\log(\mathrm{N/O}) = -1.55 \pm 0.08$ is in agreement with the average for metal-poor blue compact dwarf galaxies (Izotov & Thuan 1999).

Neon abundances are derived as $\mathrm{Ne/H} = \mathrm{ICF(Ne)(Ne^{+2}/H)}$. The ionization correction factor for neon is $\mathrm{ICF(Ne)} = \mathrm{O/O^{+2}}$. The mean $\log(\mathrm{Ne/O})$ is -0.56 ± 0.04, which is marginally consistent with the range of Ne/O values at this metallicity found by Izotov & Thuan (1999) and Garnett (2004). However, it is 0.16 dex higher than the mean value of -0.72 ± 0.06 found for blue compact galaxies by Izotov & Thuan (1999).[10] Since the [Ne III] $\lambda 3869$/[O III] $\lambda 5007$ ratio is sensitive to the reddening correction and our reddening corrections are only based on the $\mathrm{H}\alpha/\mathrm{H}\beta$ ratio, we revisited this correction. In the spectrum for H II region HM 7, higher order Balmer lines (H9, H10, and H11) were detected (Table 4). Their intensity

[9] Analytical expressions for the McGaugh calibration can be found in Kobulnicky et al. (1999).

[10] Note that part of the difference is due to a 14% difference between the ratio of the [O III] $\lambda 5007$ and [Ne III] $\lambda 3869$ emissivities used by Izotov & Thuan (1999) and that computed by the IONIC program in the NEBULAR code of Shaw & Dufour (1995). This 14% difference, which translates into a 0.06 dex difference (in the sense observed), is probably an indication of the minimum systematic uncertainty in the atomic data that are used for calculating nebular abundances (see Garnett 2004).

TABLE 8

Ionic and Total Abundances for HM 2, HM 7, HM 8, and HM9 (Grating 7)

Property	HM 2 (Grating 7)	HM 2 (Grating 11)	HM 7 (Grating 11)	HM 8 (Grating 11)	HM 9 Aperture 1 (Grating 7)	HM 9 Aperture 2 (Grating 7)	HM 9 Aperture 3 (Grating 7)
$T_e(O^{+2})$ (K)	...	<15800	15350 ± 760	...	<16500	<18500	...
$T_e(O^{+})$ (K)	...	<14100	13750 ± 680	...	<14600	<16000	...
O^{+}/H ($\times 10^5$)	...	>1.4	1.30 ± 0.21	...	>2.4	>2.0	...
O^{+2}/H ($\times 10^5$)	...	>5.3	3.92 ± 0.45	...	>2.5	>1.7	...
O/H ($\times 10^5$)	...	>6.7	5.22 ± 0.50	...	>4.9	>3.8	...
12 + log (O/H)	...	>7.83	7.72 ± 0.04 ($^{+0.05}_{-0.06}$)	...	>7.69	>7.58	...
12 + log (O/H) M91[a]	8.17	8.11	7.84	8.01	8.03	8.06	8.15
12 + log (O/H) P00[b]	7.92	7.85	7.67	8.18	7.92	7.99	8.23
Ar^{+2}/H ($\times 10^7$)	...	...	2.47 ± 0.56	...	...	...	...
Ar^{+3}/H ($\times 10^7$)	...	...	0.25 ± 0.15	...	...	...	...
ICF(Ar)	...	...	1.06	...	...	...	...
Ar/H ($\times 10^7$)	...	...	2.88 ± 0.61	...	...	...	...
log (Ar/O)	...	...	−2.25 ± 0.10	...	...	...	...
N^{+}/O^{+}	...	...	0.034 ± 0.004	...	...	...	...
log (N/O)	...	...	−1.46 ± 0.05	...	...	...	...
Ne^{+2}/O^{+2}	...	...	0.255 ± 0.027	...	...	...	...
log (Ne/O)	...	...	−0.594 ± 0.046	...	...	...	...

Notes.—Direct oxygen abundances are shown with two uncertainties. The first uncertainty is the formal uncertainty in the derivation. In parentheses is the range of possible values, expressed by the maximum and minimum values of the oxygen abundance.

[a] McGaugh (1991) bright-line calibration.

[b] Pilyugin (2000) bright-line calibration.

TABLE 9

Ionic and Total Abundances for HM 9 (Grating 11), HM 16, HM 17, HM 19, and HM 21

Property	HM 9 (Grating 11) Aperture 1	HM 9 (Grating 11) Aperture 2	HM 9 (Grating 11) Aperture 3	HM 12 (Grating 11) Obs 1[a]	HM 12 (Grating 11) Obs 2[b]	HM 16 NW (Grating 11)
$T_e(O^{+2})$ (K)	14100 ± 1000	13800 ± 1000	13300 ± 1800	...	...	<17300
$T_e(O^{+})$ (K)	12890 ± 910	12650 ± 950	12300 ± 1600	...	...	<15100
O^{+}/H ($\times 10^5$)	2.80 ± 0.68	3.10 ± 0.82	3.4 ± 1.6	...	...	>3.5
O^{+2}/H ($\times 10^5$)	5.05 ± 0.87	5.24 ± 0.98	5.5 ± 1.9	...	...	>1.5
O/H ($\times 10^5$)	7.9 ± 1.1	8.3 ± 1.3	8.9 ± 2.4	...	...	>5.0
12 + log (O/H)	7.90 ± 0.06 ($^{+0.07}_{-0.09}$)	7.92 ± 0.06 ($^{+0.08}_{-0.09}$)	7.95 ± 0.11 ($^{+0.12}_{-0.18}$)	...	...	>7.70
12 + log (O/H) M91[c]	8.04	8.04	8.01	8.16	8.00	8.21
12 + log (O/H) P00[d]	7.85	7.86	7.84	8.48	7.96	8.29
Ar^{+2}/H ($\times 10^7$)	4.2 ± 1.6	4.0 ± 1.4	4.7 ± 3.1	...	...	...
ICF(Ar)	1.50	1.48	1.48	...	...	...
Ar/H ($\times 10^7$)	6.3 ± 2.4	5.9 ± 2.1	6.9 ± 4.5	...	...	...
log (Ar/O)	−2.09 ± 0.19	−2.14 ± 0.18	−2.10 ± 0.36	...	...	...
N^{+}/O^{+}	...	0.027 ± 0.008	0.029 ± 0.007	...	...	...
log (N/O)	...	−1.57 ± 0.12	−1.53 ± 0.09	...	...	...
Ne^{+2}/O^{+2}	0.251 ± 0.034	0.276 ± 0.034	0.327 ± 0.054	...	...	...
log (Ne/O)	−0.600 ± 0.058	−0.558 ± 0.053	−0.485 ± 0.070	...	...	...

Property	HM 17 (Grating 11)	HM 19 (Grating 11) Obs 1[e]	HM 19 (Grating 11) Obs 2[f]	HM 21 (Grating 11)
12 + log (O/H) M91[c]	8.17	8.24	7.64	8.14
12 + log (O/H) P00[d]	...	8.40	8.12	8.28

Notes.—Direct oxygen abundances are shown with two uncertainties. The first uncertainty is the formal uncertainty in the derivation. In parentheses is the range of possible values, expressed by the maximum and minimum values of the oxygen abundance.

[a] Observed August 26 (UT); long slit aligned with HM 7.

[b] Observed August 28 (UT); long slit aligned with HM 19 and HM 21.

[c] McGaugh (1991) bright-line calibration.

[d] Pilyugin (2000) bright-line calibration.

[e] Observed August 27 (UT); long slit aligned with HM 16 NW and HM 16 SE.

[f] Observed August 28 (UT); long slit aligned with HM 21.

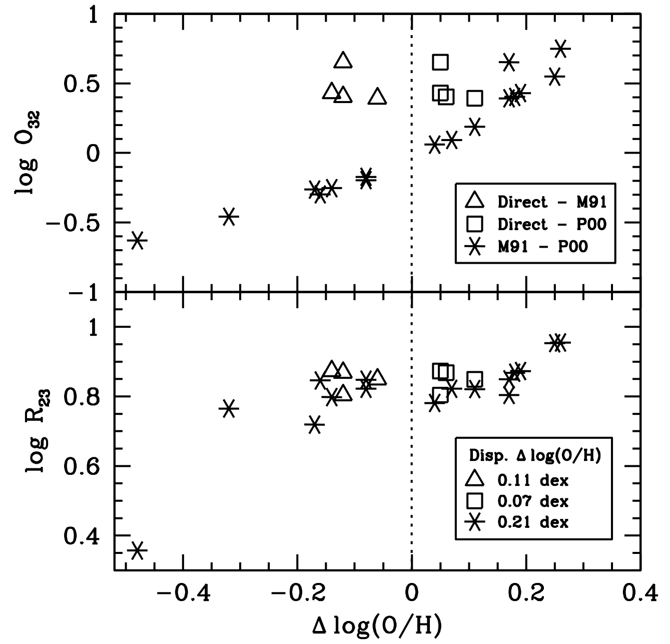

FIG. 4.—Difference in oxygen abundance from various methods vs. log O_{32} (*top*) and vs. log R_{23} (*bottom*). Each symbol represents an H II region. "Direct" denotes oxygen abundances derived from [O III] λ4363 measurements, "M91" denotes oxygen abundances derived using the bright-line method by McGaugh (1991), and "P00" denotes oxygen abundances derived using the bright-line method by Pilyugin (2000). Vertical dotted lines in both panels mark zero differences in oxygen abundance. Dispersions in abundance differences are indicated in the legend of the bottom panel. In the absence of [O III] λ4363, oxygen abundances derived with the bright-line method are accurate to within ≈0.2 dex.

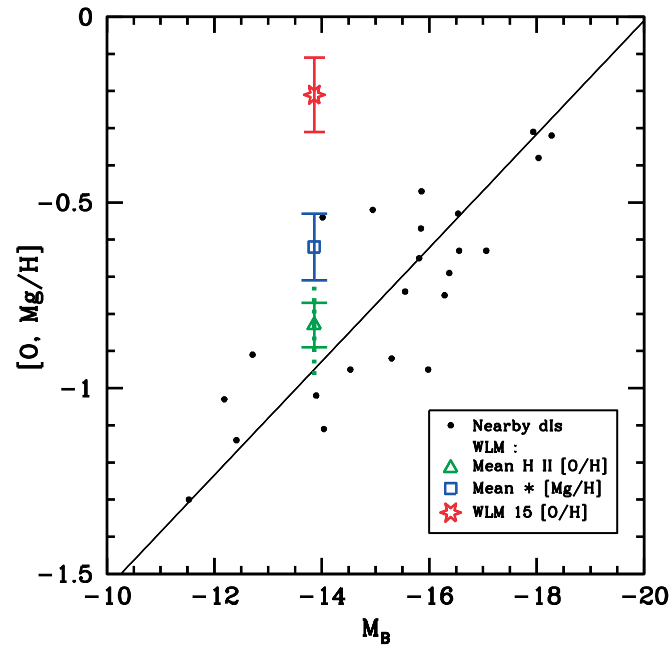

FIG. 5.—Metallicity-luminosity relationship for dwarf irregular galaxies. The filled circles represent nebular oxygen abundances for the sample of nearby dwarfs, and the solid line is the best fit (Lee et al. 2003a, 2003b). The open triangle indicates the mean nebular oxygen abundance derived in the present work; the vertical dotted line above and below the triangle marks the maximum (−0.71) and minimum (−0.98) derived values of the nebular oxygen abundance. The open square and the open star indicate the mean [Mg/H] for the two WLM supergiants and the stellar oxygen abundance for WLM 15, respectively (Venn et al. 2003; see also their Fig. 10).

ratios with respect to Hβ were found to be consistent with expected values for H II regions at a temperature of $T_e(O^{+2}) =$ 15,000 K. In the spectra (grating 11) for H II region HM 9, the closest unblended Balmer line to [Ne III] λ3869 is Hδ because H8 is blended with an adjacent helium line and Hϵ is blended with adjacent [Ne III] and helium lines. We find that corrected Hδ/Hβ and Hγ/Hβ ratios are consistent with expected Balmer ratios for $T_e(O^{+2})$ between 13,000 and 14,000 K.

Argon is more complex because the dominant ion is not found in just one zone. Ar^{+2} is likely to be found in an intermediate area between the O^+ and O^{+2} zones. Following the prescription by Izotov et al. (1994), the argon abundance was derived as $Ar/H = ICF(Ar)Ar^{+2}/H$. The ionization correction factor is given by $ICF(Ar) = Ar/Ar^{+2} = [0.15 + x(2.39 - 2.64x)]^{-1}$, where $x = O^+/O$. Our mean value of log (Ar/O) = -2.12 ± 0.12 is in agreement with the average for metal-poor blue compact dwarf galaxies (Izotov & Thuan 1999).

We note here the recent work by Moore et al. (2004), who suggested that the direct modeling of photoionized nebulae should be used to infer elemental abundances with accuracies similar to those of the observations. They showed that abundances derived from model-based ionization correction factors exceeded the range of expected errors from the original data.

5. DISCUSSION

A comparison of the present data with published spectroscopy ([O III] λ4363 detections) is shown in Table 10. Skillman et al. (1989b) obtained spectra of HM 9 and HM 2 (their H II regions 1 and 2, respectively), while Hodge & Miller (1995) reported spectra for H II regions HM 7 and HM 9. We have recomputed and added uncertainties to their published abundances in Table 10. From our measurements presented above, [O III] λ4363 was detected in H II regions HM 7 and HM 9 at a signal-to-noise ratio of about 10 σ and 5 σ, respectively. Our derived direct oxygen abundance for HM 7 is in agreement with

TABLE 10
COMPARISON WITH PREVIOUS SPECTROSCOPIC DATA

	Skillman et al. (1989b)		Hodge & Miller (1995)		Present Work	
Property	HM 2	HM 9	HM 7	HM 9	HM 7	HM 9[b]
O/H ($\times10^5$)	5 ± 3	6 ± 3	5.2 ± 0.8	6.5 ± 1.1	5.22 ± 0.50	8.16 ± 0.79
12 + log (O/H)	7.70 ± 0.30	7.78 ± 0.24	7.72 ± 0.07	7.81 ± 0.08	7.72 ± 0.04	7.91 ± 0.04
log (N/O)	...	−1.3 ± 0.2	−1.60 ± 0.15	−1.00 ± 0.24	−1.46 ± 0.05	−1.55 ± 0.08
log (Ne/O)	−0.8 ± 0.2	−0.6 ± 0.2	−0.87 ± 0.15	−0.94 ± 0.18	−0.594 ± 0.046	−0.562 ± 0.035
log (Ar/O)	...	−2.4 ± 0.2	−2.37 ± 0.14	−2.22 ± 0.18	−2.25 ± 0.10	−2.12 ± 0.12

[a] Skillman et al. (1989b) labeled their H II regions "No. 1" (HM 9) and "No. 2" (HM 2).
[b] Mean of three [O III] λ4363 measurements; see Table 9.

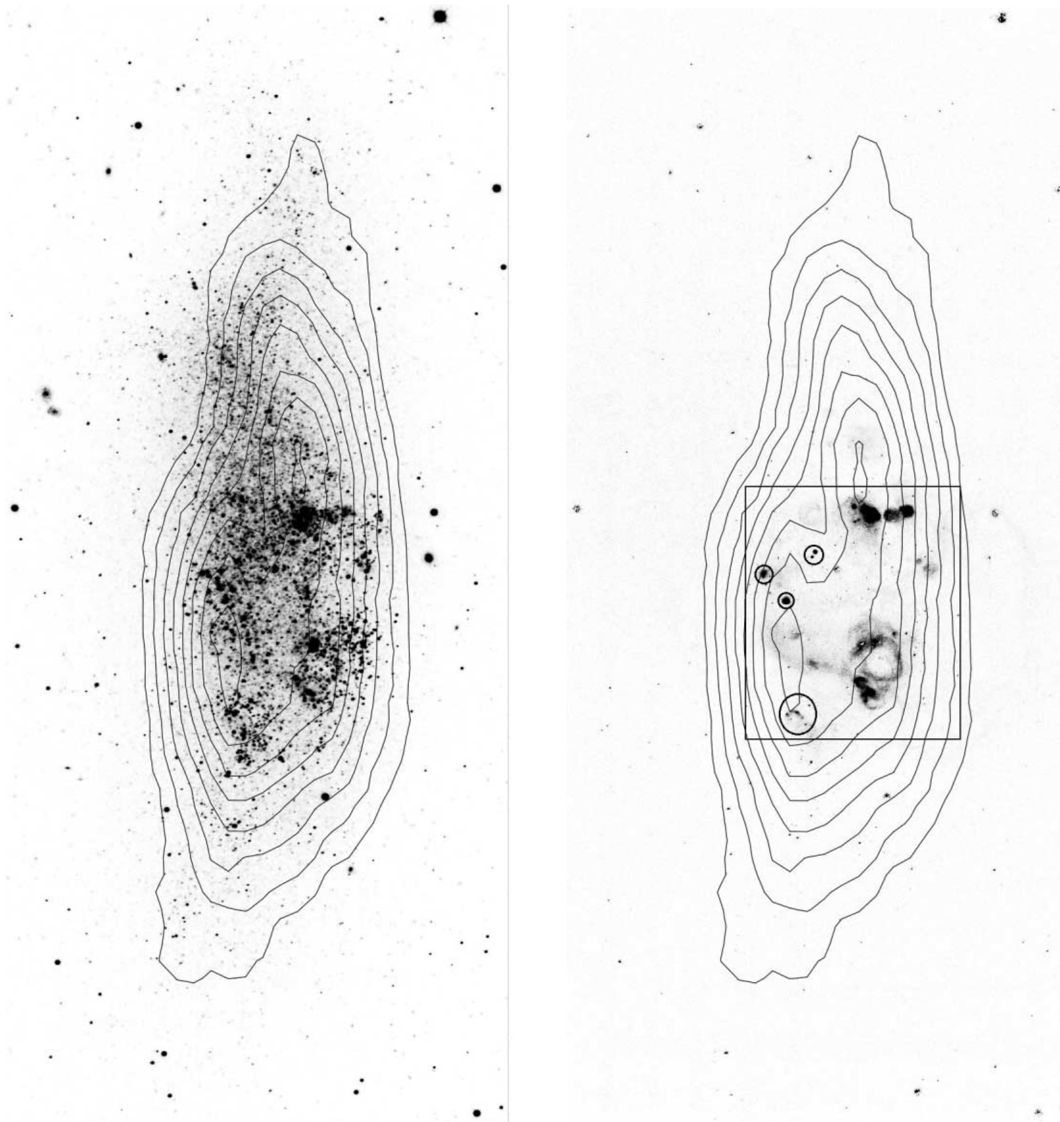

FIG. 6.—WLM in U, Hα, and H I. Dark objects on the image indicate bright sources. *Left:* H I contours superposed on a U-band image (Local Group Survey; Massey et al. 2002). *Right:* H I contours superposed on a continuum-subtracted Hα image (Local Group Survey; Massey et al. 2002). Open circles surround H II regions where the reddening, $E(B-V)$, was found to be nonzero. In both panels, north is up and east is to the left, and the field of view shown is $6'.9 \times 15'.3$. The central rectangle in the right panel encompasses the $3'.2 \times 3'.6$ area shown in Fig. 1. The figures are adapted from Jackson et al. (2004).

the value reported by Hodge & Miller (1995). The direct oxygen abundance for HM 9 is about 0.1 dex higher but consistent within errors with the values reported by Skillman et al. (1989b) and Hodge & Miller (1995). When other measurements of H II regions are included, oxygen abundances derived with bright-line methods agree with the direct values to within 0.2 dex (see Fig. 4). The present set of measurements have shown that the nebular oxygen abundances are in agreement with values published in the literature.

Figure 5 shows the metallicity-luminosity relation for dwarf irregular galaxies. We have followed Figure 10 from Venn et al. (2003) and plotted the present nebular result, the mean magnesium abundance from the two A-type supergiant stars, and the derived oxygen abundance for the supergiant WLM 15. The upper end of the range of nebular oxygen abundances derived in the present work ([O/H] between -0.98 and -0.71) is consistent with the mean stellar magnesium abundance $[\mathrm{Mg/H}] = -0.62$. However, the mean nebular oxygen abundance is 0.62 dex lower than the oxygen abundance ($[\mathrm{O/H}] = -0.21$) in WLM 15. We note that the mean stellar [Mg/H] in supergiant stars agrees with the nebular [O/H] in both NGC 6822 (Venn et al. 2001) and Sextans A (Kaufer et al. 2004). Measurements of additional supergiants in WLM will be crucial in confirming the result in WLM 15 and whether there are any spatial inhomogeneities in metallicity among stars.

Jackson et al. (2004) reported two peaks in the H I distribution; the west maximum lies just north of HM 9, whereas the second maximum lies approximately 1′ east of HM 7. Figure 6 shows that H II regions along the eastern edge of the galaxy in the vicinity of the east H I peak have nonzero reddening values derived from observed Balmer emission-line ratios. This agrees with the discovery of small regions or patches found to have redder $U-B$ and $B-V$ colors than the rest of the galaxy (Jackson et al. 2004). This is thought to be extinction internal to WLM because the foreground extinction is known to be small (see Table 1). We note that the bright H II regions (i.e., HM 7 and HM 9) on the western side of the galaxy do not exhibit any appreciable reddening. A comparison of Figures 1 and 6 shows that the two supergiant stars measured by Venn et al. (2003) are located next to the eastern H I peak. In fact, the supergiant WLM 15 with the high oxygen abundance is located (in projection) near H II region HM 18, where the average reddening was found to be $E(B-V) \gtrsim 0.5$ mag.

We have shown that the present nebular oxygen abundance agrees with previous measurements, and additional explanations are required to explain the discrepancy between the nebular and stellar oxygen abundances. Venn et al. (2003) reasoned that large changes in stellar parameters would not reconcile the stellar abundance with the nebular abundance. Three alternative scenarios were considered to explain the discrepancy: lowering the nebular abundance through dilution by the infall of metal-poor H I gas, the depletion of ISM oxygen onto dust grains, and the possibility of large spatial inhomogeneities in the metallicity. The first two scenarios were shown to be unlikely. The third scenario may be possible with the discovery of the second H I peak. However, we have shown that there are no significant variations in the nebular oxygen abundance.

Nevertheless, two questions arise. Are the nonzero reddenings measured in H II regions along the eastern side of the galaxy related to the second H I peak seen by Jackson et al. (2004)? Because of their proximity, is there any relationship between the metallicity of WLM 15 and the highly reddened H II regions in the southeast? We note that determining the oxygen abundance for the supergiant is not sensitive to internal reddening (Venn et al. 2003). On the basis of the apparent spatial correlation of the H I peak with regions of redder color, nonzero (internal) extinctions in H II regions to the east and southeast, and the location of the supergiant WLM 15, these suggest that something unusual may be happening in this more metal-rich part of the galaxy. Unfortunately, H II regions HM 18, 18a, and 18b are underluminous and exhibit very weak nebular emission; there are few additional bright H II regions in the area. Deeper spectroscopy of these H II regions may prove illuminating. However, measurements of additional blue supergiants in the center and the eastern side of the galaxy (e.g., WLM 30; Venn et al. 2003) could show whether the stellar abundances remain high with respect to the nebular values and whether the stellar abundances are also spatially homogeneous. A new search for molecular gas along the east and southeast sides of the galaxy (especially in the vicinity of WLM 15) would also be timely. While Taylor & Klein (2001) did not detect CO, their pointings missed regions of interest on the eastern side of the galaxy.

6. CONCLUSIONS

Optical spectra of 13 H II regions were obtained in WLM, and oxygen abundances were derived in nine H II regions. [O III] λ4363 was measured in bright H II regions HM 7 and HM 9. The resulting direct oxygen abundance for HM 7 is in agreement with previously published values. Our $\simeq 5\ \sigma$ detection of [O III] λ4363 in HM 9 confirms the lower signal-to-noise ratio measurements reported by Skillman et al. (1989b) and Hodge & Miller (1995). For the remaining H II regions, oxygen abundances derived with bright-line methods are accurate to about 0.2 dex. We adopt for WLM a mean nebular oxygen abundance $12 + \log(\mathrm{O/H}) = 7.83 \pm 0.06$, which corresponds to $[\mathrm{O/H}] = -0.83$, or 15% of the solar value. The upper end of the range of derived nebular oxygen abundances just agrees with the mean stellar magnesium abundance reported by Venn et al. (2003), but the present mean nebular result is still 0.62 dex lower than the oxygen abundance derived for the A-type supergiant WLM 15. Significant reddening values derived from observed Balmer emission-line ratios were found in H II regions on the eastern side of the galaxy near one of the H I peaks discovered by Jackson et al. (2004). There may be a relationship between the location of the east H I peak, regions of redder color (higher extinction), large reddenings derived from Balmer emission-line ratios in H II regions along the eastern side of the galaxy, and the location of WLM 15.

We thank the anonymous referee for comments that improved the presentation of this paper. H. L. thanks Dale Jackson for a copy of his figures. We are grateful to ESO for awarded telescope time and to Lisa Germany and the staff at ESO La Silla for their help in acquiring the spectra. H. L. and E. D. S. acknowledge partial support from NASA LTSARP grant NAG 5-9221 and from the University of Minnesota. K. A. V. thanks the National Science Foundation for support through CAREER award AST 99-84073. For their one year visit, E. D. S. and K. A. V. thank the Institute of Astronomy, University of Cambridge, for hospitality and support. This research has made use of NASA's Astrophysics Data System and of the NASA/IPAC Extragalactic Database (NED), which is operated by the Jet Propulsion Laboratory, California Institute of Technology, under contract with the National Aeronautics and Space Administration.

REFERENCES

Aller, L. H. 1984, Physics of Thermal Gaseous Nebulae (Dordrecht: Reidel)
Anders, E., & Grevesse, N. 1989, Geochim. Cosmochim. Acta, 53, 197
Asplund, M., Grevesse, N., Sauval, A. J., Allende Prieto, C., & Kiselman, D. 2004, A&A, 417, 751
Barnes, D. G., & de Blok, W. J. G. 2004, MNRAS, 351, 333
Battinelli, P., & Demers, S. 2004, A&A, 416, 111
Calura, F., Matteucci, F., & Vladilo, G. 2003, MNRAS, 340, 59
Campbell, A., Terlevich, R. J., & Melnick, J. 1986, MNRAS, 223, 811
Cardelli, J. A., Clayton, G. C., & Mathis, J. S. 1989, ApJ, 345, 245
DeRobertis, M. M., Dufour, R. J., & Hunt, R. W. 1987, JRASC, 81, 195
de Vaucouleurs, G., de Vaucouleurs, A., Corwin, H. G., Buta, R. J., Paturel, G., & Fouqué, P. 1991, Third Reference Catalog of Bright Galaxies (Berlin: Springer)
Dinerstein, H. L. 1990, in The Interstellar Medium in Galaxies, ed. H. A. Thronson & J. M. Shull (Dordrecht: Kluwer), 257
Dolphin, A. E. 2000, ApJ, 531, 804
Ferraro, F. R., Fusi Pecci, F., Tosi, M., & Buonanno, R. 1989, MNRAS, 241, 433
Garnett, D. R. 1990, ApJ, 363, 142
———. 1992, AJ, 103, 1330
———. 2004, in Cosmochemistry: The Melting Pot of the Elements, XIII Canary Islands Winter School of Astrophysics, ed. C. Esteban, R. J. García-López, A. Herrero, & F. Sánchez (Cambridge: Cambridge Univ. Press), 171
Gilmore, G., & Wyse, R. F. G. 1991, ApJ, 367, L55
Grebel, E. K., Gallagher, J. S., & Harbeck, D. 2003, AJ, 125, 1926
Grevesse, N., & Sauval, A. J. 1998, Space Sci. Rev., 85, 161
Hodge, P. W., Dolphin, A. E., Smith, T. R., & Mateo, M. 1999, ApJ, 521, 577
Hodge, P. W., & Miller, B. W. 1995, ApJ, 451, 176 (HM95)
Hunter, D. A., Hawley, W. N., & Gallagher, J. S. 1993, AJ, 106, 1797
Izotov, Y. I., & Thuan, T. X. 1999, ApJ, 511, 639
Izotov, Y. I., Thuan, T. X., & Lipovetsky, V. A. 1994, ApJ, 435, 647
Jackson, D. C., Skillman, E. D., Cannon, J. M., & Côté, S. 2004, AJ, 128, 1219
Jacoby, G. H., & Lesser, M. P. 1981, AJ, 86, 185
Kaufer, A., Venn, K. A., Tolstoy, E., Pinte, C., & Kudritzki, R. P. 2004, AJ, 127, 2723
Kobulnicky, H. A., Kennicutt, R. C., Jr., & Pizagno, J. L. 1999, ApJ, 514, 544
Kobulnicky, H. A., & Skillman, E. D. 1996, ApJ, 471, 211
———. 1997, ApJ, 489, 636
Krawchuk, C. A. P., McCall, M. L., Komljenovic, M., Kingsburgh, R., Richer, M. G., & Stevenson, C. 1997, in IAU Symp. 180, Planetary Nebulae, ed. H. J. Habing & H. J. G. L. M. Lamers (Dordrecht: Kluwer), 116
Lee, H. 2001, Ph.D. thesis, York Univ.
Lee, H., Grebel, E. K., & Hodge, P. W. 2003a, A&A, 401, 141

Lee, H., McCall, M. L., Kingsburgh, R., Ross, R., & Stevenson, C. C. 2003b, AJ, 125, 146
Lee, H., McCall, M. L., & Richer, M. G. 2003c, AJ, 125, 2975
Lee, H., & Skillman, E. D. 2004, ApJ, 614, 698
Lennon, D. J., & Burke, V. M. 1994, A&AS, 103, 273
Martin, N. F., Ibata, R. A., Bellazzini, M., Irwin, M. J., Lewis, G. F., & Dehnen, W. 2004, MNRAS, 348, 12
Massey, P., Hodge, P. W., Holmes, S., Jacoby, G., King, N. L., Olsen, K., Smith, C., & Saha, A. 2002, BAAS, 34, 1272
Matteucci, F. 2003, Ap&SS, 284, 539
McCall, M. L., Rybski, P. M., & Shields, G. A. 1985, ApJS, 57, 1
McGaugh, S. S. 1991, ApJ, 380, 140
———. 1994, ApJ, 426, 135
McLaughlin, B. M., & Bell, K. L. 1993, ApJ, 408, 753
Melotte, P. J. 1926, MNRAS, 86, 636
Minniti, D., & Zijlstra, A. A. 1996, ApJ, 467, L13
———. 1997, AJ, 114, 147
Moore, B. D., Hester, J. J., & Dufour, R. J. 2004, AJ, 127, 3484
Olive, K. A., & Skillman, E. D. 2001, NewA, 6, 119
Osterbrock, D. E. 1989, Astrophysics of Gaseous Nebulae and Active Galactic Nuclei (Mill Valley: University Science Books)
Pagel, B. E. J., Edmunds, M. G., Blackwell, D. E., Chen, M. S., & Smith, G. 1979, MNRAS, 189, 95
Pilyugin, L. S. 2000, A&A, 362, 325
Pradhan, A. K. 1976, MNRAS, 177, 31
Prochaska, J. X., Gawiser, E., Wolfe, A. M., Castro, S., & Djorgovski, S. G. 2003, ApJ, 595, L9
Rejkuba, M., Minniti, D., Gregg, M. D., Zijlstra, A. A., Victoria Alonso, M., & Goudfrooij, P. 2000, AJ, 120, 801
Richer, M. G., & McCall, M. L. 1995, ApJ, 445, 642
Rodríguez, M. 2003, ApJ, 590, 296
Sandage, A., & Carlson, G. 1985, AJ, 90, 1464
Schlegel, D. J., Finkbeiner, D. P., & Davis, M. 1998, ApJ, 500, 525
Shaw, R. A., & Dufour, R. J. 1995, PASP, 107, 896
Skillman, E. D. 1989, ApJ, 347, 883
Skillman, E. D. 1998, in Stellar Astrophysics of the Local Group: VIII Canary Islands Winter School of Astrophysics, ed. A. Aparicio, A. Herrero, & F. Sánchez (Cambridge: Cambridge Univ. Press), 457
Skillman, E. D., Côté, S., & Miller, B. W. 2003a, AJ, 125, 610
Skillman, E. D., Kennicutt, R. C., Jr., & Hodge, P. 1989a, ApJ, 347, 875
Skillman, E. D., Terlevich, R., & Melnick, J. 1989b, MNRAS, 240, 563 (STM89)
Skillman, E. D., Tolstoy, E., Cole, A. A., Dolphin, A. E., Saha, A., Gallagher, J. S., Dohm-Palmer, R. C., & Mateo, M. 2003b, ApJ, 596, 253
Storey, P. J., & Hummer, P. J. 1995, MNRAS, 272, 41
Taylor, C. L., & Klein, U. 2001, A&A, 366, 811
Tolstoy, E., & Venn, K. A. 2005, in Proc. Joint Discussion 15 of the 2003 IAU, ed. O. Engvold (San Francisco: ASP), in press (astro-ph/0402295)
Tolstoy, E., Venn, K. A., Shetrone, M. D., Primas, F., Hill, V., Kaufer, A., & Szeifert, T. 2003, AJ, 125, 707
Tomita, A., Ohta, K., Nakanishi, K., Takeuchi, T., & Saito, M. 1998, AJ, 116, 131
van Zee, L., Salzer, J. J., Haynes, M. P., O'Donoghue, A. A., & Balonek, T. J. 1998, AJ, 116, 2805
van Zee, L., Skillman, E. D., & Haynes, M. P. 2004, AJ, 128, 121
Venn, K. A., Irwin, M., Shetrone, M. D., Tout, C. A., Hill, V., & Tolstoy, E. 2004a, AJ, 128, 1177
Venn, K. A., Tolstoy, E., Kaufer, A., & Kudritzki, R. P. 2004b, in Origin and Evolution of the Elements, ed. A. McWilliam & M. Rauch (Pasadena: Carnegie Observatories), http://www.ociw.edu/ociw/symposia/series/symposium4/proceedings.html
Venn, K. A., Tolstoy, E., Kaufer, A., Skillman, E. D., Clarkson, S. M., Smartt, S. J., Lennon, D. J., & Kudritzki, R. P. 2003, AJ, 126, 1326
Venn, K. A., et al. 2001, ApJ, 547, 765
Whiting, A. B., Hau, G. K. T., & Irwin, M. 1999, AJ, 118, 2767
Wiese, W. L., Fuhr, J. R., & Deters, T. M. 1996, Atomic Transition Probabilities of Carbon, Nitrogen, and Oxygen: A Critical Data Compilation (J. Phys. Chem. Ref. Data Monogr. 7; Melville: AIP)
Wolf, M. 1910, Astron. Nachr., 183, 187
Yanny, B., et al. 2003, ApJ, 588, 824 (erratum 605, 575 [2004])
Zucker, D. B., et al. 2004a, ApJ, 612, L117
———. 2004b, ApJ, 612, L121